Chapter 2

Biopolymer adsorption on differently shaped brush-modified surfaces

2.1 Introduction

The structural modification of microparticles (MPs) has become increasingly important in the biomedical field, especially in targeted drug and cell delivery, self-assembly, and diagnostics [108–111]. Recent research has shown that the size, shape, and structure of MPs significantly affect their physiological interactions and biological performance [73,112], including margination, circulation half-life, and opsonization [113–116]. In addition to the commonly used spherical MPs, there is a growing use of MPs with different shapes such as cups, discs, rods, tubes, and ellipsoids for controlled drug delivery systems [73,112,117,118]. For example, hemispherical-shaped particles have been demonstrated to have superior cellular uptake [113,119] and margination ability in the microvasculature compared to spheres [113]. On the other hand, rod-like and disc-shaped particles have shown better adherence to the microvascular network due to their strong binding affinity [120,121]. Therefore, controlled surface modification of the particles is crucial for various biomedical applications [7,40,73,122–124]. Various techniques such as solvent evaporation [119], vapor deposition [125], mini-emulsion

[126,127], and microfluidics [128] are utilized for the controlled surface modification of the particles, such as polymeric cup-shaped particles.

The immobilization of biopolymers, such as enzymes, on solid surfaces has gained significant attention in various fields such as biocatalysis, food processing, drug and textile manufacturing, and biosensors [129–131]. This has sparked interest in finding more efficient ways to utilize biopolymers and expand their applications [20,40,74,132,133]. Furthermore, immobilizing biopolymers on insoluble solid particles enhances rapid arrest and controlled quenching of reaction kinetics due to easier extraction of solid surface-bound biopolymers from the solution [20,40,74,132–138]. Immobilizing biopolymers on solid particles has improved the stability and reusability of biopolymers against changes in pH, solvent, and temperature during successive chemical reactions [139–141]. This immobilization process has significant medical and industrial applications [139]. Additionally, surface-modified solid particles with polyelectrolyte ATRP-brush, such as poly(DMAEMA), can immobilize a considerable amount of biopolymer through electrostatic adsorption in their brush morphology due to the high charge density [141–143]. Brush-modified surfaces have shown promising results in immobilizing biopolymers due to their unique structures [140,141,143].

Ifra and her colleagues have recently demonstrated differently-shaped MP modifications using the electrojetting technique [40,73,123,124]. Specifically, a blend of polylactide (PLA) and poly(methylmethacrylate- co-2-(2-bromopropionyloxy) ethyl methacrylate), i.e., poly(MMA-co-BEMA) in a 3 : 1 ratio [123] is used to prepare different MPs. To modify the surface, they synthesized poly(DMAEMA) brushes using a grafting from approach at the initiator (BEMA molecule) embedded surfaces through ATRP [40,73,123] with DMAEMA monomer in water ($pH = 7$). The brush grafting density was controlled by changing the initiator concentration on the surfaces. Varying the polymerization time produced ATRP brushes of different lengths, thereby controlling the surface charge of the fabricated surface. Consequently, the

efficiency of electrostatic adsorption of the biopolymer (α - Glucosidase) onto the surface of a brush-modified particle was enhanced [40,140,141].

The experimental findings by Ifra and co-workers [40] are better understood through a DPD simulation study, which provides insights into the underlying physical phenomena at the atomic level. In DPD, the system evolution follows Newton's equation of motion [22,23,35,37]. The advantage of using the DPD technique is well-known for preserving the hydrodynamic behavior of modeled polymeric solutions, melts, and biopolymers in crowded and confined environments, which is crucial for estimating the system's dynamic behavior [144,145]. Hence, DPD is a very effective particle (DPD bead) simulation technique [22,23]. It is extensively used to model various types of free radical polymerization processes and to study the effect of shape and size on the dynamics of complex soft materials [35,37].

This chapter introduces a general DPD model that focuses on surface fabrication using surface-initiated ATRP-brush growth on differently shaped surfaces such as cups, spheres, and disc/rectangular, and the subsequent adsorption of biopolymers on these modified surfaces. Our simulation includes a comparative study that varies the percentage of initiator concentration and polymerization time to adjust the brush density and length and analyses their impact on biopolymer adsorption. We also compare these findings with experimental results. The biopolymer is represented as a linear chain (similar to a polymer chain) of soft beads connected by harmonic bonds.

In this work, we have organized our content as follows: In section 2.2, we provide details of the system's computational model and simulation parameters. In section 2.3, we discuss the results of brush growth from the initiators implanted at three different surfaces using surface-initiated ATRP in the solvent. We also analyze the adsorption of biopolymers at the brush-modified cup surface (CS), spherical surface (SS), and flat rectangular surface (RS) particles for various biopolymer concentrations in the solution. Finally, in section 2.4, we conclude the work with a summary.

2.2 Methodology and model parameter

We have used the DPD simulation technique, which is a coarse-grained MD approach where beads symbolize a molecule or a cluster of particles [22,23]. Further details of the DPD simulation are provided in section 1.4. In this section, we exclusively discuss the model parameters.

The interaction parameters have been set as follows: $a_{ii} = 25$ (in reduced DPD units) for compatible beads, and $a_{ij} = 60$ for any two incompatible beads. These choices were made with careful consideration, including the compressibility of water when coarse-graining ten water molecules into a single bead, as discussed by Groot [22]. We will be providing the remaining parameters shortly [35]. In the reduced DPD units, r_c, m, and k_BT are all set to 1.0, with k_BT establishing the model's normal energy scale [22,27]. To effectively integrate the equations of motion, we employ the modified Velocity-Verlet algorithm [22,33]. The simulation time step is to $\Delta t = 0.02\tau$, where τ is the characteristic time scale. The total bead number density in the simulation box is set to $\rho = 3$, which is a reasonable choice for DPD simulation of liquids [22,23]. The selected coarse-graining parameters consist of time scale values of $\tau \approx 8.3$ ps and length scale values of $r_c \approx 0.97$ nm.

We have used a bead-spring model to represent the polymer chains [43]. The harmonic bond potential (E_b) connects neighboring DPD beads with $k_b = 128$ and $r_0 = 0.5$ [29]. Additionally, the angle potential provides stiffness to the polymer chain with $k_a = 5$ and $\theta_0 = 180$ [29,43,45]. More details about this bead spring model are given in section 1.4.2.

2.2.1 Preparation of microparticles

In our study, we used the DPD simulation technique to model three different surfaces as rigid bodies: a cup, a sphere, and a rectangular surface. This modeling work was complemented by experimental work. The MPs were made of PLA blended with poly(MMA-co-BEMA) in a 3 : 1 ratio in the experiments [40]. The poly(BEMA) compound initiated the ATRP process, with

DMAEMA monomers present in the solution to modify the surface. The cup and spherical-shaped MP were created using double-layered DPD beads on the vertices of a geodesic grid formed by subdividing an icosahedron [48]. The inner and outer radii of the cup-shaped surface were set to $R_{in} = 7.7r_c$ and $R_{out} = 8.0r_c$. The cup-shaped MP contained 1962 beads (N_{CS}) with a volume fraction (ϕ_{CS}) of 5.23×10^{-3}, while the spherical-shaped MP comprised 3924 beads (N_{SS}) with a volume fraction (ϕ_{SS}) of 1.04×10^{-2}. The rectangular-shaped MP were modeled as a double-layered flat structure consisting of 1960 beads (N_{RS}) with a volume fraction (ϕ_{RS}) of 5.23×10^{-3}, arranged in a regular lattice structure with a lattice constant of $0.5r_c$. Each layer contained an equal number of beads, and the size of the rectangular MP was $17.5r_c \times 14r_c$ with a thickness of $dz = 0.5r_c$. The number density of beads was kept sufficiently high ($\rho_m = 11$) in each layer of CS, SS, and RS to prevent the penetration of ATRP-brush and other beads.

In our experimental research [40,123,124], we have identified that only a fraction of the poly(BEMA) molecules on the surface of the MPs serve as initiators in the solution. To accurately represent this in our simulation, we have meticulously chosen a specific proportion of MP beads to act as initiator beads. Notably, we randomly selected the initiator beads for the CS and RS from the particle surface, while for the SS, we exclusively chose them from the outer surface. Note that the flat surface is a disk-shaped particle in the experiment, whereas we model it as a rectangular-shaped particle in the simulation. We have carefully considered three different initiator values: $N_i = 20$, 50, and 100, equating to 1%, 2.5%, and 5% of MP beads, respectively. These values correspond to the appropriate volume fractions of 1.33×10^{-4}, 2.66×10^{-4}, and 5.3×10^{-5}. The outcome of this arrangement is the growth of polymer brushes (B) from the surface during polymerization. Additionally, the MPs are insoluble in the solvent (s), with their interaction set at $a_{ms} = 45$. Taking into account the slightly incompatible interaction between MP bead (m) and monomer bead (M), we have established $a_{mM} = 35$, and set its interaction with the polymer brush as $a_{mB} = 35$.

2.2.2 Surface fabrication of microparticles via ATRP

In our work, we modify the MPs via the ATRP process; the description of polymerization is given in sections 1.6.1 and 1.7. We chose a monomer volume fraction of $\phi_M = 1.0 \times 10^{-1}$ ($N_M = 37500$) to grow the polymer brushes in the system. The interaction parameters between the monomer, ATRP brush, and solvent are set to $a_{Ms} = a_{Bs} = 25$ in DPD units. This is because the monomer and ATRP brushes are hydrophilic and compatible with solvent beads, so we assigned an interaction value of 25 for both with the solvent. The experimental results [73,123] show that the poly(DMAEMA) brushes carry a positive charge in a pure solvent (water at $pH \approx 7$) due to the protonated amino groups. Therefore, we have taken the interaction between the monomer and brush beads, $a_{MB} = 25$. Therefore, the brushes are well dispersed in the solvent due to the long-range electrostatic repulsion. We are investigating the brush-biopolymer affinity to study biopolymer adsorption within the brush matrix. However, explicitly solving electrostatic interactions in the DPD framework [146–148] is computationally expensive for large systems [39], even with the recent parallel Poisson solver [39,148]. Therefore, the explicit use of charge distribution in the DPD simulation approach for biological systems is rare [39,149–151]. We set the DPD interaction parameter between brush-brush to $a_{BB} = 27$ to prevent brush aggregation.

2.2.3 Modeling the biopolymer adsorption

The biopolymer, α-glucosidase enzyme, is modeled similarly to a polymer using the bead spring model. The biopolymer is modeled as a linear chain of N_b DPD beads connected by harmonic bonds with an elastic constant $k_b = 128$ and an equilibrium bond distance $r_0 = 0.5$ [152]. The angle potential coefficient between two consecutive bonds along the biopolymer chain is $k_a = 5$, with an equilibrium angle $\theta_0 = 180$ between successive bonds. The mass of each biopolymer bead is set to 1.0 in the reduced DPD unit. We study biopolymer adsorption at three different biopolymer concentrations: $c_b = 2\%N$ ($\phi_b = 2.0 \times 10^{-2}$), $4\%N$ ($\phi_b = 4.0 \times 10^{-2}$) and,

$c_b = 8\%N$ ($\phi_b = 8.0 \times 10^{-2}$). The corresponding number of DPD beads are $N_b = 7500$, 15000, and 30000, respectively. Further, to examine the effect of biopolymer length on adsorption at fabricated surfaces, we choose $l_b = 25, 10$, and 1.

The biopolymers (α-glucosidase [40]) are chemically compatible with the solvent and have negatively charged molecules. We have found effective DPD interaction parameters between the biopolymer and biopolymer beads, like in a brush scenario, where we set $a_{bb} = 27$ to prevent their aggregation. The negatively charged biopolymers will be attracted to the positively charged brush beads, so we have set the interaction parameters between these beads to $a_{Bb} = 15$ to account for this favorable interaction. We will enhance brush dispersion in the solvent by explicitly modeling long-range electrostatic interactions instead of relying on short-range effective DPD interactions. This means that even though direct electrostatic interactions can improve biopolymer adsorption, the results of this study will not change.

In this study, we used a simulation box with dimensions of $50r_c \times 50r_c \times 50rc$. The total number of beads in the box is 375,000, with an overall number density set to $\rho = 3r_c^{-3}$. We applied periodic boundary conditions along the x and y axes and used amorphous solid walls [37] to confine the z-direction. The walls have a height of $h = 1$, and bead density of $\rho_w = 3$, and a corresponding volume fraction of $\phi_w = 4.0 \times 10^{-2}$. To prevent particles from penetrating the walls, bounce-back boundary conditions [105] were implemented at the fluid-wall interface [153]. We also considered the repulsive interaction between the wall and other beads, which is characterized by an interaction parameter of $a_{wj} = 60$.

The solvent volume fraction within the simulation box is fixed as follows: $\phi_s \approx 8.3 \times 10^{-1}$ for $\phi_b \approx 2.0 \times 10^{-2}$, $\phi_s \approx 8.1 \times 10^{-1}$ for $\phi_b \approx 4.0 \times 10^{-2}$, $\phi_s \approx 7.7 \times 10^{-1}$ for $\phi_b \approx 8.0 \times 10^{-2}$. The interaction parameters for all DPD beads are summarized in Table 2.1.

The DPD simulation begins by placing the microparticle in a simulation box and randomly distributing the monomers and solvent. The system is equilibrated for $t = 1 \times 10^5$ simulation time steps before polymerization processes may begin. To create MP surfaces with variable

Table 2.1: The interaction parameter a_{ij} used in the simulation for different DPD beads.

a_{ij}	w	s	m	M	B	b
$Wall(w)$	25	60	60	60	60	60
$Solvent(s)$		25	45	25	25	25
$Microparticle(m)$			25	35	35	20
$Monomer(M)$				25	25	25
$Brush(B)$					27	15
$Biopolymer(b)$						27

brush lengths, the ATRP brush is allowed to grow at three time intervals: $t_{BG} = 400, 800$, and 1500 simulation steps. Next, we introduce the biopolymers in the solution containing fabricated MPs and their adsorption is observed for up to $t_{bA} = 3000$ simulated time steps.

2.3 Result and discussion

2.3.1 Simulation study

We initiated a study to explore the polymer brush modification of a cup particle's surface. The initiators are evenly distributed on both the inner and outer surfaces of the cup particle. We considered three different initiator concentration to understand their effects on surface fabrication: $c_i = 1\%$, 2.5%, and 5% of N_{cs}. We initiate surface modification by starting the ATRP reaction with the monomer and solvent in the system. In order to assess the extent of monomer participation in the polymerization process and to analyze the polymerization kinetics, we initially plot a graph of the monomer conversion ($\text{Conv}_M = [M]_{rt} / [M]_0$) and the reaction rate $\log([M]_0 / [M]_{ut})$ as functions of time t_{BG} in Fig. 2.1. In this context, $[M]_0$ represents the total monomer concentration in the system, while $[M]_{rt}$ and $[M]_{ut}$ denote the amounts of reacted and unreacted monomer in the system, respectively, at time t_{BG} following the polymerization process.

We polymerized the cup surface using three different initiator concentrations: $c_i = 1.0\%$, $c_i = 2.5\%$, and $c_i = 5.0\%$. The polymerization proceeded for a time up to $t_{BG} = 1500$. The monomer conversion rates were approximately 6% for $c_i = 1\%$ (black curve), 13% for $c_i = 2.5\%$ (red curve), and 21% for $c_i = 5\%$ (green curve) within the time $t_{BG} = 1500$. We then analyzed the linear monomer conversion in ATRP process at early up to $t_{BG} = 1500$, as shown in Fig. 2.1(a). The plot tends towards unity ($\text{Conv}_M \to 1.0$) when all monomers have participated in the polymerization process at later times (shown in Fig. 2.2(a)).

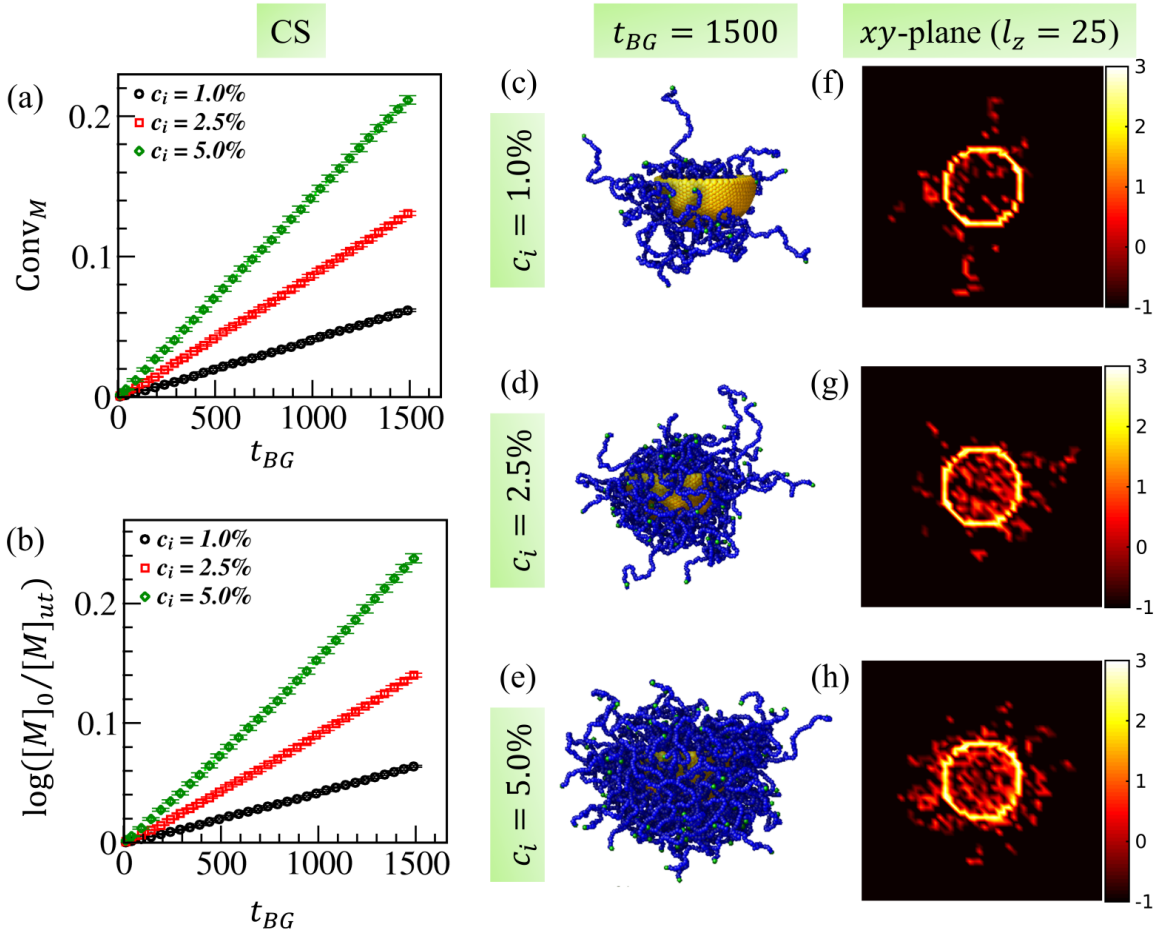

Fig. 2.1: (a) The graph shows the monomer conversion $(Conv_M)$ over time (t_{BG}) for three different initiator concentrations: $c_i = 1.0\%$, 2.5%, and 5.0%. (b) The plot illustrates the change in the monomer conversion rate, $\log([M]_0/[M]_{ut})$ over time. (c-e) display ATRP brush-modified cup surfaces at different c_i up to $t_{BG} = 1500$. (f-h) show the corresponding cross-section plots at $l_z = 25$, indicating brush density variation around CS. The color bar is at the extreme right.

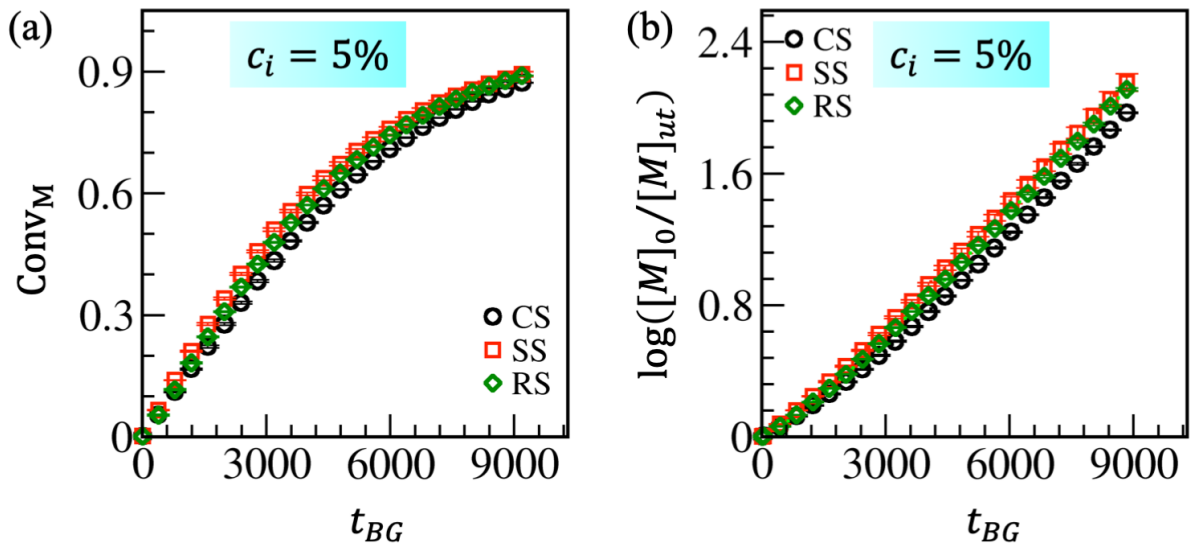

Fig. 2.2: The figure shows the comparison of the temporal variation of monomer conversion $Conv_M$ in (a) and the natural logarithm of the ratio of initial monomer concentration to monomer concentration at time t, $\log([M]_0/[M]_{ut})$, in (b) at the surfaces of the cup (CS) in black, spherical surface (SS) in red, and rectangular surface (RS) in green curves for a $c_i = 5.0\%$ initiator concentration embedded on their surfaces.

The natural logarithm of the ratio of initial concentration to unreacted concentration at time t, $\log([M]_0/[M]_{ut})$, exhibits a nearly linear relationship with time for all c_i values, as shown in Fig. 2.1(b). This trend continues into the later stages, as illustrated in Fig. 2.2(b), suggesting that our model accurately represents the pseudo-first-order kinetics, which is commonly observed in live radical polymerization [36,37,71]. Snapshots of the fabricated CS for the ATRP-brush growth up to $t_{BG} = 1500$ at various initiator concentrations are presented in Figs. 2.1(c-e). The variation in brush density around the CS in the xy-plane at $l_z = 25$, corresponding to Figs. 2.1(c-e), is shown in Figs. 2.1(f-h). The figures display the ATRP-brush density in the red region and the CS cross-section in the yellow circle. These snapshots illustrate that as the monomer conversion increases (approximately 21%) based on $c_i = 5.0\%$ at the CS, the brush density also increases. The presence of initiators on the inner surface of the CS is further confirmed by the red region within it (yellow circle).

The size of the macromolecule is determined by two parameters: the radius of gyration and the hydrodynamic radius. The radius of gyration (R_g) [105,106] is calculated $R_g =$

$\left(\frac{1}{N}\sum_i \langle r_i^2 \rangle\right)^{1/2}$ as a function of time (t_{BG}) for different initiator concentrations (c_i) 1.0%, 2.5%, and 5.0%. The results of the radius of gyration are shown by the black, red, and green curves in Fig. 2.3(a). The plots in Fig. 2.3(a) demonstrate that the size of the macromolecule increases over time as the degree of polymerization $(Conv_M)$ increases for all concentrations. However, at a higher concentration of 5.0%, the $Conv_M$ is higher at a specific duration of polymerization, resulting in larger values of R_g observed over time, as indicated by the curves in Fig. 2.3(a).

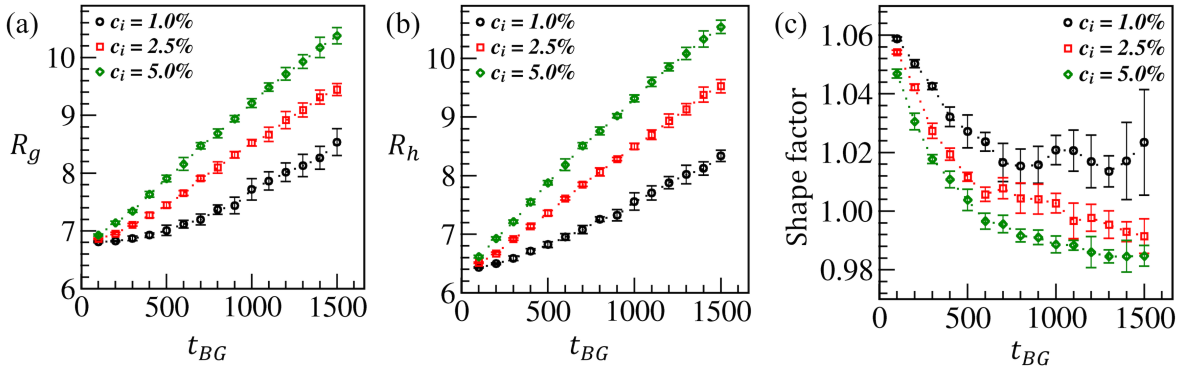

Fig. 2.3: Radius of gyration R_g (a), the hydrodynamic radius R_h (b), and the shape factor $\rho_{sf} = R_g/R_h$ (c) are shown with the ATRP brush growth time t_{BG} for CS. The curves in black, red, and green represent for the initiator concentrations of $c_i = 1.0\%$, 2.5%, and 5.0%, respectively, embedded on the CS surface.

The ATRP process involves adding one monomer at a time to grow a polymer chain, resulting in a nearly monodispersed growing chain [50,51,69,71]. When the initiator concentration is low, the length of each polymer chain (degree of polymerization) is longer compared to a given monomer concentration at any point during the polymerization process. Based on the results displayed in Fig. 2.1, the approximate brush length l_B is $n_B r_0$, where n_B represents the number of monomers in the brush. For the initiator concentrations $c_i = 1.0\%$, 2.5%, and 5.0%, the n_B values are 115, 100, and 86 respectively, at the brush growth time $t_{BG} = 1500$. In this case, the average is taken over five ensembles. Due to the positively charged DPD beads, the polymer brushes are repulsive with CS and themselves. Consequently, the ATRP polymer brushes are more swollen and extended in the solvent for $c_i = 5.0\%$ than for $c_i = 1.0\%$. As a result, the radius of gyration R_g is higher for $c_i = 5.0\%$.

We calculate hydrodynamic radius R_h [42,105–107], which represents the size of a solvated molecule more accurately. Therefore, it is a more suitable biological parameter for determining the size of a molecule in its environment. The R_h of a modified particle is measured by assuming that the brush embedded on its surface moves through the solution and is resisted by the solvent viscosity. The hydrodynamic radius formulation is given by $\frac{1}{R_h} = \frac{1}{2N^2}\left\langle \sum_{i\neq j} \frac{1}{r_{ij}} \right\rangle$. The average across five ensembles is indicated by the angular brackets, and r_{ij} represents the distance between beads i and j of the polymer brush and CS (N). As the brush density increases at CS, R_h also increases linearly with time, approximately the same magnitude as R_g in Fig. 2.3(a). The larger R_h for $c_i = 5.0\%$ can be explained by greater brush swelling with increased initiator concentration.

To characterize the shape of the macromolecule, we calculate the shape factor, which is the ratio of R_g and R_h. The global polymer structures have a shape factor of about 0.775 [105,106]. However, if the macromolecule deviates from a globular shape to a non-globular or elongated shape, the ratio of R_g to R_h attains higher values as R_g becomes larger than R_h. The hollow sphere has a shape factor of approximately 1.0. Initially, the brush growth is minimal, so the shape factor for the modified CS at this stage is estimated to be within the range of 1.05 to 1.065 for all c_i values as shown in Fig. 2.3(c). However, as time progresses, the ATRP-brush-modified CS tends to take on a more globular shape, causing the shape factor to decrease. At later times, the shape factor is slightly lower (approximately 0.985) for $c_i = 5.0\%$ compared to the other two values (see Fig. 2.3(c)). However, when we allow the brush growth to continue for a much longer time until the degree of conversion reaches 90%, the fabricated MP attains a shape factor of approximately 0.94 (this result is not displayed here due to brevity).

Next, we calculate the radial distribution function (RDF), denoted as $g(r) = \rho_{lB}/\rho_B$, to illustrate the distribution of polymerized brush beads tethered at a radial distance, r, from the CS beads. The local brush density is represented by $\rho_{lB}(r) = n_{lB}(r)/V_{sh}$, while the total brush density is denoted by $\rho_B = N_B/V$. Here, $\rho_{lB}(r)$ stands for the local number of brush beads,

$n_{lB}(r)$, in a shell of volume V_{sh} at a distance r from the microparticle bead, where N_B is the total number of brush beads and V is the total volume of the box.

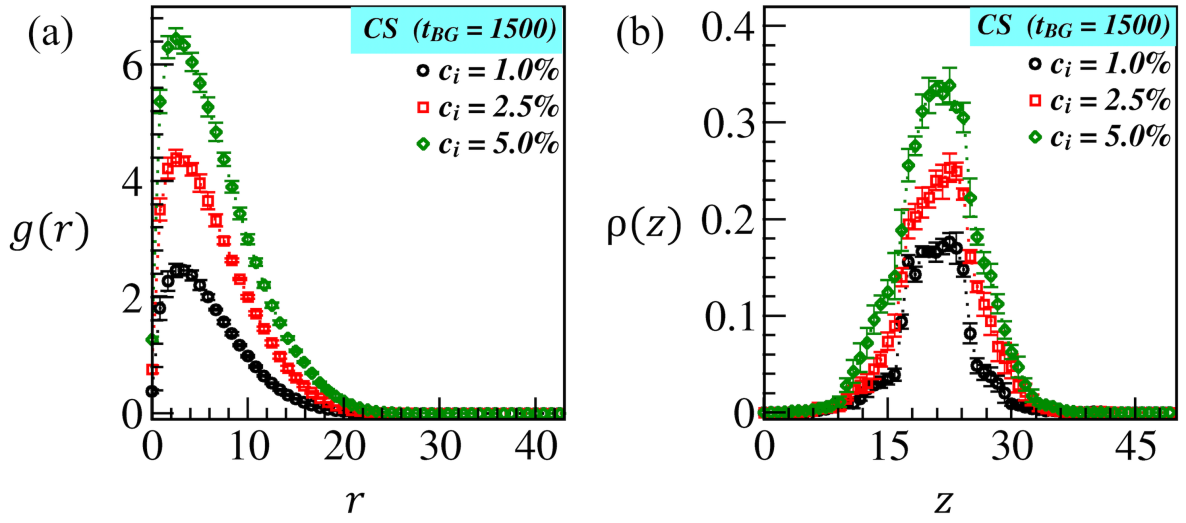

Fig. 2.4: The radial distribution function with radial distance, $g(r)$ vs. r is shown in (a) and (b) the density distribution, ρ_z, depicts the distribution of the grown ATRP-brushes along the z-direction at time $t_{BG} = 1500$ at CS for various initiator concentrations: $c_i = 1.0\%$ (black symbols), 2.5% (red symbols), and 5.0% (green symbols), corresponding to the snapshots shown in Fig. 2.1(c-e).

The RDF plot illustrates the variation in distribution for three different values of c_i, represented by the black, red, and green symbols in Fig. 2.4(a). The larger peak width and height of the green curve confirm that brush beads are more tightly bound around CS at $c_i = 5.0\%$, attributed to a higher monomer conversion, in comparison to $c_i = 1.0\%$ and 2.5%. Due to a higher monomer conversion at $c_i = 5.0\%$ compared to $c_i = 1.0\%$ and 2.5%, we observed a larger peak width and height for the green curve, validating that the brushes are more tightly bound around CS for $c_i = 5.0\%$. The plot in Fig. 2.4(b) shows the number density of brush beads along the transverse $z-$direction, denoted as $\rho(z)$. The curves corresponding to different c_i values confirm that more brush beads are concentrated around CS $(10 < z < 30)$ at $c_i = 5.0\%$ compared to $c_i = 1.0\%$ and $c_i = 2.5\%$. Overall, an increase in the initiator concentration leads to noticeable brush swelling, which could enhance the diffusion of biopolymers into the brush matrix, thereby enabling immobilization.

To understand the impact of ATRP-brush growth on surface modification and biopolymer adsorption, we will examine two other different surfaces, SS and RS. We will start by analyzing the physical attributes associated with the structural modifications of SS and RS with CS. Then, we will compare the fabrication of SS and RS with CS, focusing on the polymerization up to the same simulation time steps for $c_i = 5.0\%$. This comparison aims to showcase the substantial swelling of brush-modified CS due to brush growth up to $t_{BG} = 1500$ at $c_i = 5.0\%$.

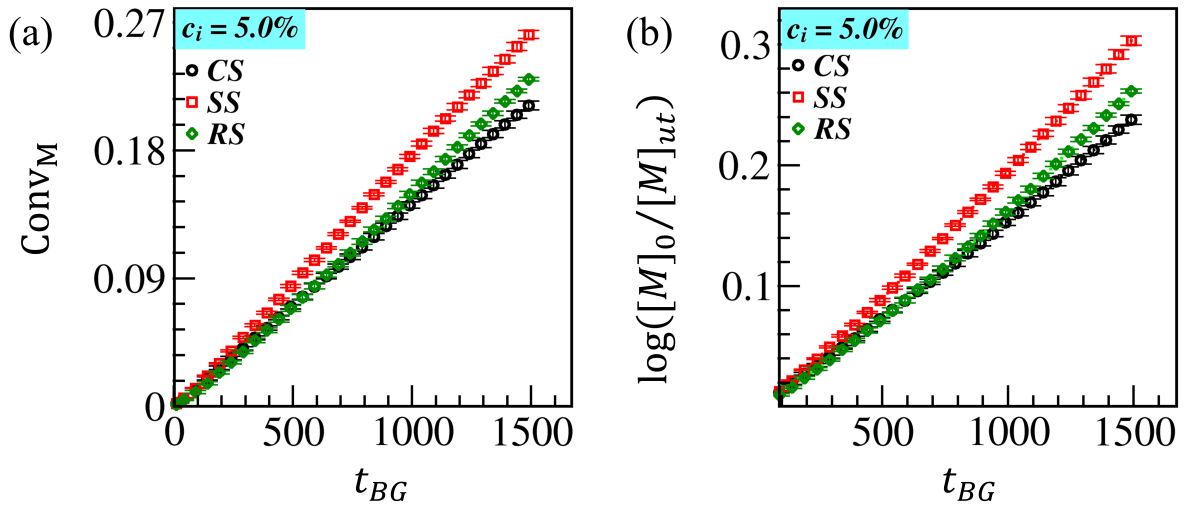

Fig. 2.5: Comparison of the temporal variations of $Conv_M$ (a) and $\log([M]_0/[M]_{ut})$ (b) at the cup surface (CS, black curve), spherical surface (SS, red curve), and rectangular surface (RS, green curve) for $c_i = 5.0\%$.

We plot $Conv_M$ and $\log([M]_0/[M]_{ut})$ for SS and RS with time in Fig. 2.5 and compared the outcomes with CS. The initiators are evenly distributed at both the surfaces of RS and only at the outer surface of SS. The ATRP brushes are grown up to $t_{BG} = 1500$ during surface modification. At early stages ($t_{BG} \lessapprox 350$), we observed that the $Conv_M$ for SS (red curve) is slightly higher than RS (green curve) and CS (black curve). However, as time progresses, the difference becomes more pronounced, as shown in Figs. 2.5(a) and 2.5(b), due to higher monomer accessibility to active radicals tethered at a larger outer surface of SS compared to the case of CS and RS. The propagation reaction ($Conv_M$) at RS initially grows at a similar rate to CS during the early period ($t_{BG} \lessapprox 1000$). However, a slightly higher conversion is obtained

for RS beyond this time. In the case of RS, monomers are equally accessible to initiators on both sides, allowing initiators/active radicals equal access to the monomers. Brush growth on the outer CS can proceed at the same pace as on the SS; however, monomers are less accessible to initiators on the inner concave surface of the CS. The effective rate of chain propagation at CS is balanced by achieving lower monomer conversion compared to RS and SS. Fig. 2.5(b) shows that the propagation reaction rate $\log([M]_0/[M]_{ut})$ at different surfaces varies linearly with time (t_{BG}), indicating the expected first-order reaction kinetics.

We examined the morphology of fabricated CS, SS, and RS due to ATRP-brush growth at various polymerization times, $(t_{BG} = 400)$ (Fig. 2.6(a-c)), 800 (Fig. 2.6(d-f)), and 1500 (Fig. 2.6(g-i)) at $(c_i = 5.0\%)$. In Fig. 2.5(a), it is shown that (Conv_M) at CS, SS, and RS for $(t_{BG} = 1500)$ are approximately 23%, 26%, and 24%, respectively. The estimated brush length is $(l_B \simeq n_B r_0)$, where $n_B \simeq 79$, 97, and 86 are the number of polymerized beads per brush chain, bounded at CS, SS, and RS, respectively.

The monomer conversion is approximately the same on all surfaces at $t_{BG} = 400$, resulting in almost the same brush length: $l_B \simeq 21r_0$ for CS and RS, and $l_B \simeq 26r_0$ for SS. However, the brush length l_B grows with time and differs somewhat on different surfaces due to varied monomer conversion, as shown in Fig. 2.5. The estimated brush lengths for polymerization up to $t_{BG} = 800$, are $l_B \simeq 41r_0$, $53r_0$, and $43r_0$ at CS, SS, and RS, where $\text{Conv}_M \simeq 11\%$, 14%, and 12%, respectively. Figs. 2.6(j-l) depict the brush density fluctuation around MP surfaces in the xy-plane at $l_z = 25$, corresponding to Figs. 2.6(g–i). The yellow color depicts the cross-section of different MPs, whereas the red area shows the ATRP-brush density.

At $c_i = 5.0\%$, we compared the shape and size of ATRP-brush modified differently shaped particles. In Fig. 2.7(a) we displayed R_g as a function of t_{BG}. The difference in R_g values is due to the varied MP structures; SS has a greater R_g than CS and RS. However, later, these two surfaces (CS and RS) maintained equal growth in R_g with time, with a minor advancement for RS at late times due to greater Conv_M (shown in Fig. 2.5). Despite a significant Conv_M at SS

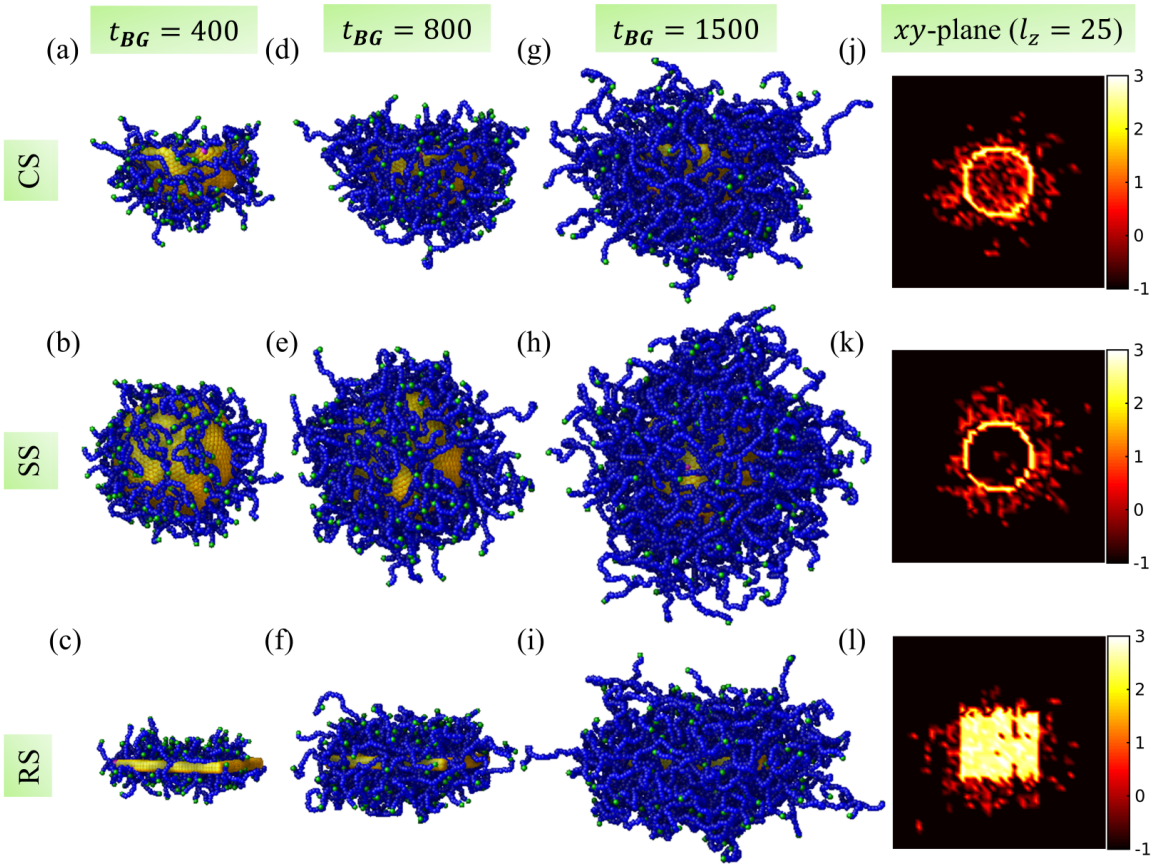

Fig. 2.6: The ATRP brush-modification of CS, SS, and RS for $c_i = 5.0\%$ up to the brush growth (polymerization) time $t_{BG} = 400$ (a–c), 800 (d–f), and 1500 (g–i). (j–l) The brush density variation in the xy cross-section at $l_z = 25$ corresponds to the snapshots in (g–i).

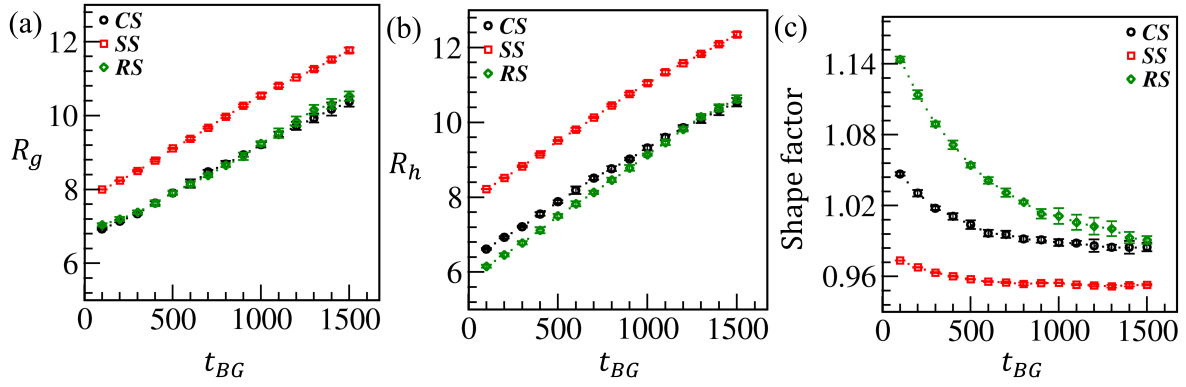

Fig. 2.7: Comparison of the (a) radius of gyration R_g, (b) hydrodynamic radius R_h, and (c) shape factor ρ_{sf} vs. the polymerization time t_{BG} for the brush-modified CS (black curve), SS (red curve), and RS (green curve), respectively, at $c_i = 5\%$.

(as stated in Fig. 2.5), the first surge in R_g persists until late times. The hydrodynamic radius (R_h) for the modified surfaces changes linearly with time, much as R_g, as seen in Fig. 2.7(b). In order to compare and analyze the changes in the shape of modified MPs over time, we have plotted the shape factor in Fig. 2.7(c). Initially, the shape factor (ρ_{sf}) is highest for RS and lowest for SS, when the $Conv_M$ is minimal. However, as the polymerization progresses, the shape factor for CS and RS becomes comparable. Throughout the entire polymerization period considered here, the shape factor for SS remains the lowest.

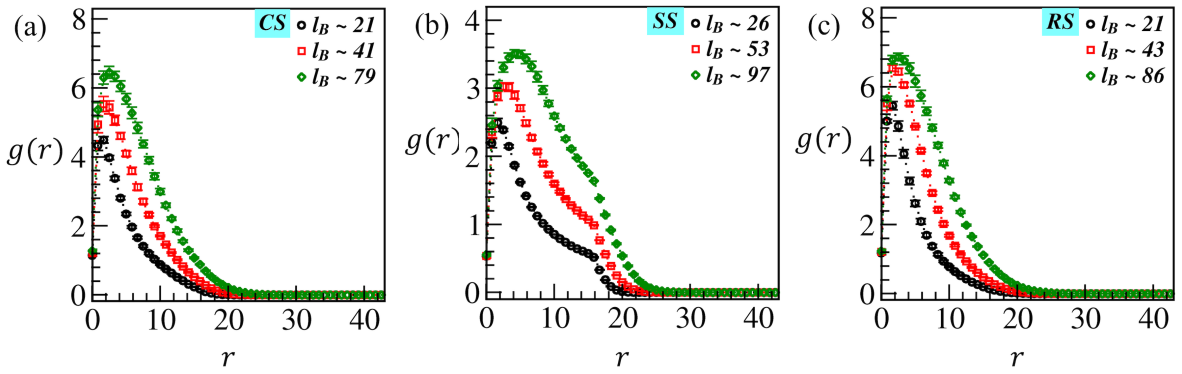

Fig. 2.8: Comparison of the radial distribution function (RDF) $g(r)$ of ATRP brushes around (a) CS, (b) SS, and (c) RS at different brush lengths observed at various polymerization times for $c_i = 5\%$.

We compare the function $g(r)$ for the ATRP brushes at a concentration of $c_i = 5.0\%$ for three different brush lengths assessed at $t_{BG} = 400$, 800, and 1500 around CS in Fig. 2.8(a), SS in Fig. 2.8(b), and RS in Fig. 2.8(c). We previously discussed and estimated the corresponding brush lengths at each surface. Fig. 2.8 illustrates that the peak height shifts to a higher position for the modified particles and increases with brush length, indicating an increase in the local brush density (ρ_{lB}). Consequently, the brushes and MP surfaces are more closely bound. The broadening of the RDF width with r confirms the spreading of growing brush chains. As $r \to \infty$, the local brush density and $g(r) \to 0$ vanishes. Following the previous observations as depicted in Figs. 2.5-2.7, the fluctuation of $g(r)$ for CS and RS is relatively similar. However, $g(r)$ for RS has a slight edge over CS, as shown in Fig. 2.8(a) and 2.8(c). The peak of $g(r)$ for SS is lower than for CS and RS, as depicted in Fig. 2.8(b). The smaller n_{lB} per shell and

greater N_{ss} (equal to $2 \times N_{cs}$ or $2 \times N_{Rs}$) may be due to the hollow core of the spherical MP, resulting in lower $\rho_{lB}(r)$. There is also a sharp increase at $r \approx 2R_0$ because SS has a hollow core impermeable to other beads, including the brush beads.

As the polymerization continues, the density of grafted brushes and surface charges increases. The incompatible interaction between the brush beads causes the brushes to swell and stretch ($a_{BB} = 27$). Additionally, a highly favorable interaction ($a_{Bb} = 15$) between the swollen brush and the negatively charged biopolymers ($a_{bb} = 27$) allows the biopolymers to reach the brush area and become adsorbed.

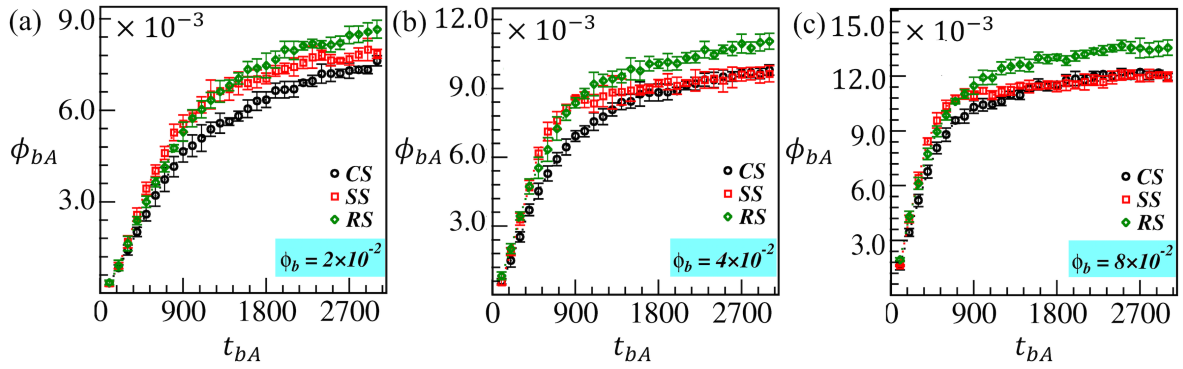

Fig. 2.9: The estimated fraction of adsorbed biopolymers, ϕ_{bA}, is shown for brush-modified CS (black symbols), SS (red symbols), and RS (green symbols) with different biopolymer fractions: (a) $\phi_b = 2 \times 10^{-2}$, (b) $\phi_b = 4 \times 10^{-2}$, and (c) $\phi_b = 8 \times 10^{-2}$ in the solution with $c_i = 5\%$. The adsorption process is monitored for $t_{bA} = 3000$.

We introduce equilibrated biopolymer chains of length $l_b = 25$ into the solution for a time of $t_{bA} = 3000$ and examine the adsorption at various brush-modified surfaces. We compare the fraction of biopolymer adsorbed with time in Figs. 2.9(a-c) using fabricated CS (black curve), SS (red curve), and RS (green curve) in the presence of different fractions of biopolymers, $\phi_b = 2 \times 10^{-2}$, 4×10^{-2}, and 8×10^{-2}, respectively. We observed that for a brief initial time ($t_{bA} \lesssim 300$), the biopolymers are adsorbed inside the brush region on various brush-modified surfaces at approximately the same rate. However, over time, ϕ_{bA} for SS is growing faster than for CS and RS, up to $t_{bA} \lesssim 900$. This result is consistent for every biopolymer concentration employed in the simulation. Furthermore, it seems pretty evident as the brush length (l_B) and

the radius of gyration (R_g) are prominent for SS due to higher monomer conversion than for CS and RS.

To compute ϕ_{bA}, we count the number of biopolymer beads within R_g of modified MPs and then scale it with the total number of beads (N) in the system. An interesting observation is that for $t_{bA} > 900$, the ϕ_{bA} curves for RS show a gradual crossover to a significantly larger value (green curves in Fig. 2.9) compared to the other two surfaces for all biopolymer concentrations (ϕ_b). As ϕ_b values increase, as shown in Figs. 2.9(b-c), the crossover becomes more noticeable. In contrast, the ϕ_{bA} data for the SS (red curve) and CS (black curve) converge to almost the same lower value (steady-state value) for a given ϕ_b at late times. The red curve (ϕ_{bA} for SS) approaches the steady-state faster than the black curve (for CS) at a relatively higher ϕ_b. At later times, the lower ϕ_{bA} at SS could be due to a larger volume of the swollen brush region caused by a greater brush length (l_B) resulting from higher monomer conversion at SS. The larger volume implies a more porous brush region around SS. Therefore, the biopolymers can more easily diffuse into the brush matrix due to a favorable interaction ($a_{Bb} = 15$) between the brush and biopolymer beads. It is important to note that biopolymers are negatively charged molecules. As a result, some biopolymers can quickly diffuse out of the brush region after relatively quick initial adsorption due to an unfavorable interaction ($a_{bb} = 27$) between the biopolymer beads. Therefore, the number of trapped biopolymers within fabricated SS is relatively small than in the case of RS.

Let us analyze the adsorption of biopolymers on various modified surfaces using thermodynamic terminology. In the early stages, there is low brush density, indicating a favorable interaction between the brush and biopolymer, leading to biopolymer adsorption driven mainly by enthalpy. The Gibbs free energy ($\Delta G = \Delta H - T\Delta S$) has a minimal entropic impact. Similar trends are observed in biopolymer adsorption (refer to Fig. 2.9) and monomer conversion up to $t_{bA} \simeq 900$ (refer to Fig. 2.5(a)). A gradual increase in brush entropy, which is higher for the spherical particle, suggests increased free space for the brush to move around due to the

increase in monomer conversion. An enthalpic penalty, or positive enthalpy change, typically follows an increase in entropy. Over time, the enthalpic penalty increases as biopolymers diffuse into the brush area, due to slightly unfavorable interactions between the brush-brush and biopolymer-biopolymer. This leads to a decrease in binding affinity for all three surfaces over time, and biopolymer adsorption saturates at later stages. Consequently, due to its lower entropy gain (or higher binding affinity), a flat surface (indicated by the green curve in Fig. 2.5) shows more enzyme adsorption than the spherical surface, despite having a smaller surface area and somewhat lower monomer conversion compared to the other two surfaces. Fig. 2.9 illustrates how the green curve progressively shifts to a higher saturation value at later time.

Further, we studied surface-initiated ATRP brushes that grew up to $t_{BG} = 400$, 800, and 1500 for each surface in this study, with $c_i = 5\%$ and $\phi_b = 8 \times 10^{-2}$, to demonstrate the impact of brush lengths on biopolymer adsorption. Brush lengths are measured in units of r_0. The corresponding brush lengths are approximately $l_B = 21$, 41, and 79 for CS, $l_B = 26$, 53, and 97 for SS, and $l_B = 21$, 43, and 86 for RS. First, we plot $g(r)$ vs. r in Fig. 2.10 at $t_{bA} = 3000$ to analyze biopolymer adsorption at various brush lengths. This is primarily done to illustrate the radial distribution of biopolymers within the brush region. The biopolymer chain length $l_b = 25$ is used in this instance. The graphs with black, red, and green curves display the increasing order of $g(r)$ data for different brush lengths. In Fig. 2.10(a), it is evident that the strength and position of the $g(r)$ peak enhanced for CS and expanded as l_B increased. This indicates that with a longer brush length, a higher percentage of biopolymers evenly diffused into the brush region. Figs. 2.10(b–c) demonstrate similar behavior for SS and RS. As displayed in Fig. 2.8(b), the absence of biopolymer molecules within the hollow SS results in a sudden increase in $g(r)$ for SS at $r \approx 2R_0$. In Figs. 2.10(d-f), we plot ϕ_{bA} vs. t_{bA}, the black, red, and green curves reveal that biopolymer adsorption increases with l_B. Fig. 2.10(f) for RS, there is a higher proportion of adsorbed biopolymer compared to Figs. 2.10(d–e) for CS and SS, which is similar to Fig. 2.9. After an initial growth in ϕ_{bA}, the data saturate to a specific value for each

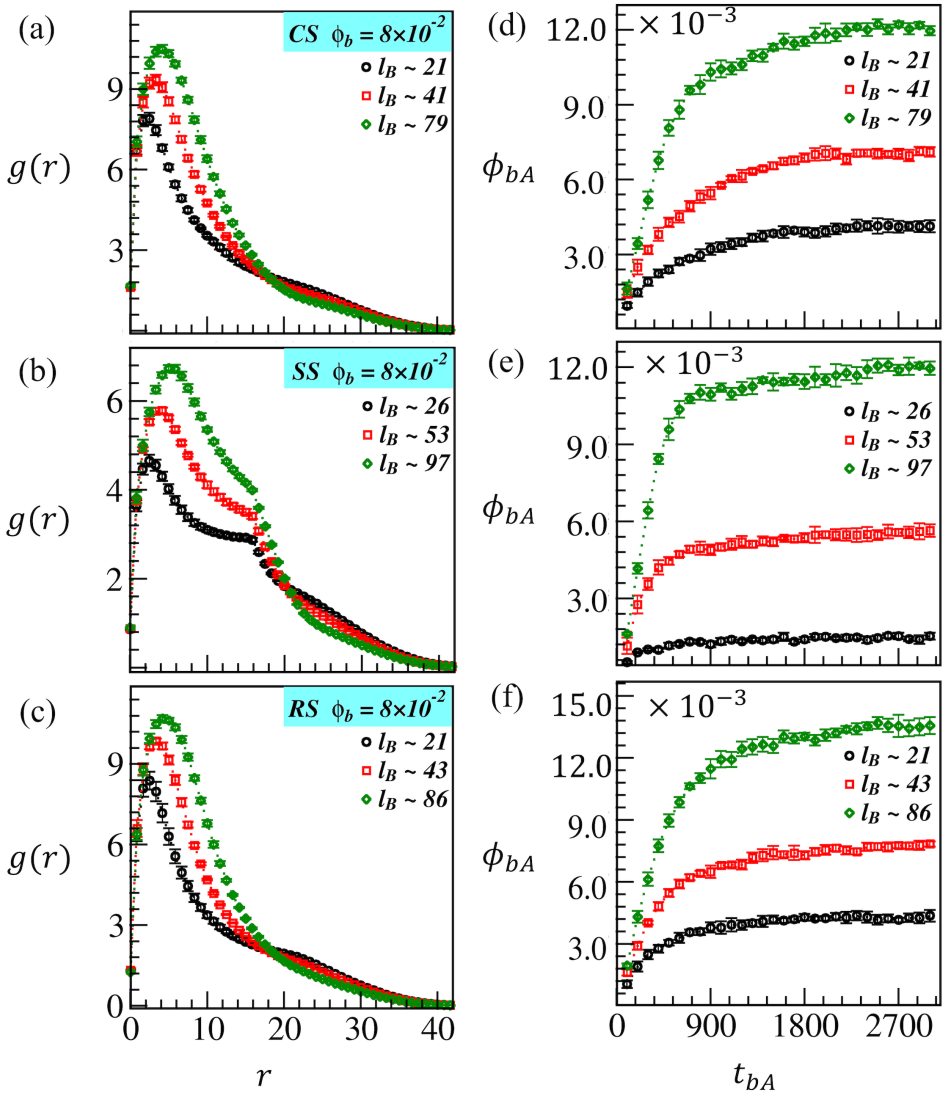

Fig. 2.10: Comparison of the biopolymers adsorption for different brush lengths grown up to $t_{BG} = 400$, 800, and 1500 on CS, SS, and RS, respectively. The corresponding brush lengths are shown in the legend. The adsorption is for each brush length until $t_{bA} = 3000$. (a–c) display $g(r)$ vs. r for the biopolymers around CS, SS, and RS beads, respectively. (d–f) show the temporal variation in the adsorbed fraction of biopolymers, ϕ_{bA}.

brush length at late times; this behavior remains the same for all the modified surfaces. The associated data saturates early, and the adsorption is negligible for the shorter brushes.

In Fig. 2.11, it is evident that the amount of adsorption on brush-modified surfaces is greatly influenced by the length of the biopolymer (l_b). To investigate this, we studied biopolymers with three different chain lengths ($l_b = 1$, 10, and 25). We monitored their adsorption up to

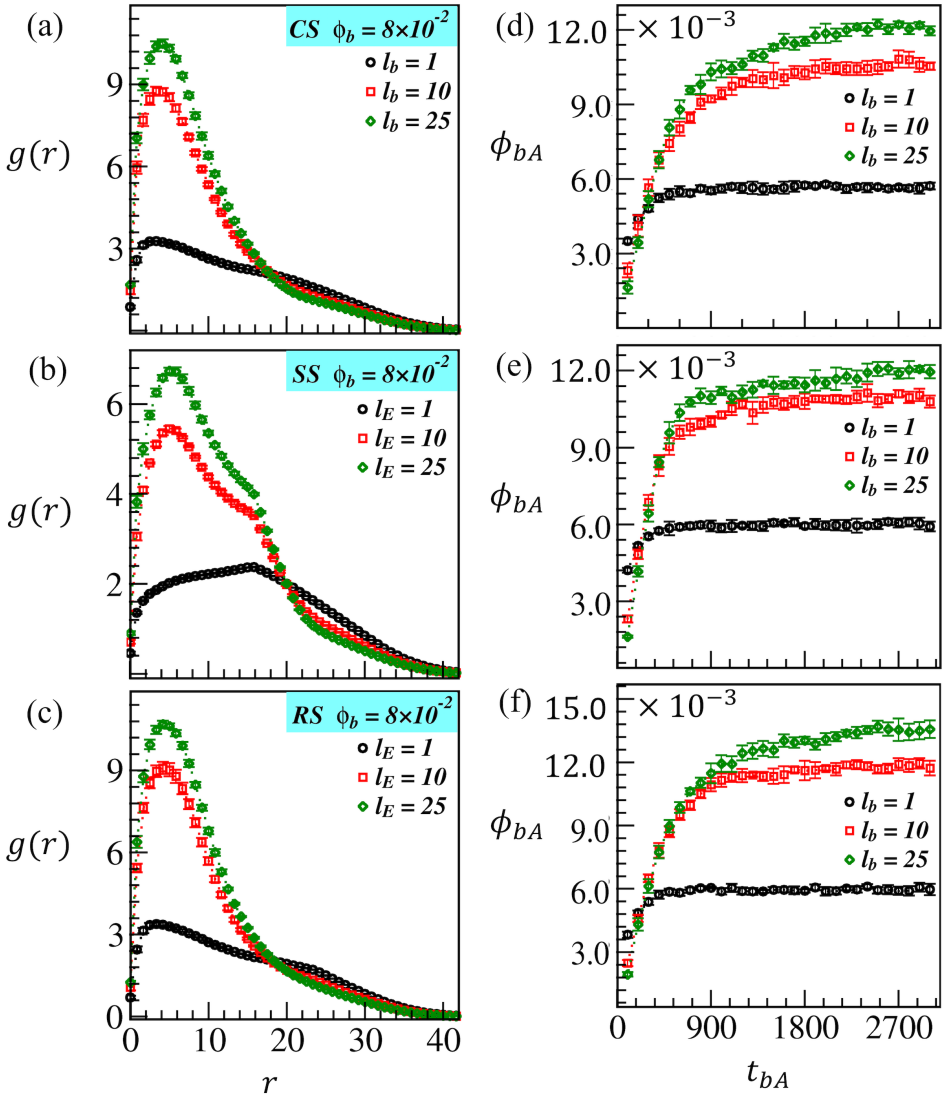

Fig. 2.11: Assessment of the adsorption of biopolymers with different chain lengths: $l_b = 1$ (black curve), $l_b = 10$ (red curve), and $l_b = 25$ (green curve) on brush-modified surfaces: CS, SS, and RS. The adsorption process continued for $t_{bA} = 3000$. (a–c) show the RDF plot $g(r)$ vs. r, while (d–f) display the temporal variation of the adsorbed fraction of biopolymers, ϕ_{bA}.

$t_{bA} = 3000$ at $\phi_b = 8 \times 10^{-2}$. The black, red, and green symbols in Fig. 2.11 represent the $g(r)$ vs r plots and ϕ_{bA} vs. t_{bA} curves. These illustrate the amount and distribution of biopolymers adsorbed in the ATRP-brush matrix on CS, SS, and RS. For $c_i = 5\%$, the brushes were allowed to grow on these surfaces until $t_{BG} = 1500$. The graphs show that adsorption is more for longer biopolymer chains, regardless of the type of surface. The RDF curves in Figs. 2.11(a-c) shows

for $l_b = 25$ and 10, the green and red curves show that biopolymers are more densely packed around the surfaces due to the higher peak strength at lower r. When we coarse-grain it with a single bead $(l_b = 1)$, the biopolymer is equally dispersed across a broad range of r from the surface beads and loosely confined around the modified surfaces, as indicated by the black $g(r)$ curves.

The curves in Fig. 2.11(d–f) demonstrate that ϕ_{bA} saturates to a finite value, i.e., the biopolymer adsorption attains a steady-state value, for all the cases studied here within the adsorption time $t_{bA} = 3000$. Similar to the findings for $l_b = 25$ (refer to Figs. 2.9 and 2.10), ϕ_{bA} is higher at RS $(\phi_{bA} \approx 11.6 \times 10^{-3})$ compared to CS and SS with $(\phi_{bA} \approx 10.6 \times 10^{-3})$ for $l_b = 10$. It is worth noting that when the biomolecule size l_b decreases, it reaches its steady-state value earlier. Additionally, the difference in ϕ_{bA} values at different surfaces becomes less significant. Therefore, for all the modified surfaces (indicated by the black curves in Fig. 2.11(d-f)), $\phi_{bA} \approx 6.0 \times 10^{-3}$ for $l_b = 1$. The quick movement of smaller molecules into and out of the brush region can be explained by the diffusion coefficient $D \sim N_b^{-1}$, where N_b is the number of beads in a biopolymer chain. Because longer biopolymer chains diffuse more slowly, it takes longer for them to become fully saturated compared to smaller chains. However, when longer biopolymer chains are diffused into the brush matrix due to strong favorable interaction, they tend to get trapped due to structural constraints.

2.4 Conclusion

In summary, we used the DPD approach to create a versatile simulation model for fabricating microparticles with different shapes using surface-initiated ATRP brush grafting. Specifically, we looked at modifying initiator-embedded cups, spheres, and flat (rectangular/disc-shaped) surfaces. We then performed a comparative study of biopolymer adsorption on these brush-modified surfaces to appreciate the critical chemical and physical processes happening at the microscopic level.

Independent of the shape of MPs, the monomer conversion is enhanced with the increase of initiator concentration for a fixed period of ATRP; thus, for any given surface, we marked an increase in the radius of gyration and hydrodynamic radius under the same conditions. The reaction rate kinetics depicted a linear brush growth, as expected for any typical living radical polymerization process, thus validating the chemical kinetics of our simulation model. We observed that polymerization reduced the shape factor for all the fabricated surfaces at a fixed initiator concentration. Due to the initial structural constraint of the rectangular surface, we examined a more significant change for this surface. This further led to forming a more globular shape with a polymer brush. The radial distribution function compellingly revealed a consistently uniform distribution of ATRP brushes near the surface for all initiator concentrations, with markedly greater density at higher initiator concentrations. The gradual decrease in brush density with distance convincingly affirmed the swelling of the brushes in the solvent.

In our research, we have examined how biopolymers adhere to surfaces modified with a brush-like coating. We observed that the adsorption of biopolymers increased under the following conditions: (i) when the brush length on a surface with a fixed initiator concentration increased, (ii) when the initiator concentration was increased, resulting in surfaces with a higher grafting density and more swollen brush morphology, and (iii) when the biopolymer concentration increased. We also noted that the adsorption of biopolymers continued for an extended period, eventually reaching a steady state or saturation point in most cases. Importantly, when adsorption reached saturation later, flat surfaces (rectangular or disc-shaped) could adsorb more biopolymers than other surfaces having nearly the same adsorption. Our experimental results confirmed this, particularly when considering disc-shaped flat surface particles, cups, and spherical particles.

We have achieved a significantly high biopolymer loading for longer biopolymer chains on all surfaces. Notably, the modified flat surface exhibited the highest adsorption, consistent with

other cases. Conversely, when the small biopolymer molecules were coarse-grained as a single bead, we observed a notably low and nearly equal loading on all the modified surfaces. Overall, our simulation data aligned with the experimental results. These exciting findings could open up new possibilities in shaping complex soft materials, which is crucial for various applications in the biomedical field. For example, the role of shape and surface chemistry is vital in advanced drug delivery and the development of biomedical devices through cell-material interactions.